Concurrent Dual and Triple Band Square Ring Resonator Base-Band Filter using Metal-Insulator-Metal for Plasmonic Applications

Surendra Kumar Bitra[*] and Sridhar Miriyala

Department of Electronics and Communication Engineering
KLEF, Vaddeswaram, Andhra Pradesh, 522503, India
bitrasurendrakumar@gmail.com*, sridhar.m@kluniversity.in

Abstract ─ Ring resonators are capable of providing high-quality factors with low insertion loss, which are the factors for considering it as a potential technique of guiding signal in the nanometer wavelengths. In this paper, a Nanoplasmonic configuration of a resonator comprising of the square ring known as Square Ring Resonator (SRR) is designed and analyzed for multiple band characteristics. The performance analysis of two different structures of the square ring resonators are presented in terms of the simulation reports like reflection and transmission coefficients, and field distribution plots. The designed Band Pass Filter (BPF) expressed excellent performance in the optical bands and hence are best suitable for Photonic Integrated Circuit (PIC) applications.

Index Terms ─ BPF, dual band, MIM, PIC, SRR, surface plasmons, triple band.

I. INTRODUCTION

Surface plasmons (SPs) have drawn awareness in the past few years due to their excellent functionality in plasmonic Metal-Insulator-Metal (MIM) waveguides. They have the potential to manipulate and guide the light at sub-wavelength because of the strong localization of surface plasmon polaritons (SPPs) at the metal dielectric interface [1-2]. Nanowires [3], nanoparticles [4], metal wedges [5], metallic grooves [6], MIM waveguides [7] are designed and developed based on the above characteristics. Moreover, among these, MIM waveguides have exceptional and significant advantages such as miniaturization and ultra-high density photonic integrated circuits (PICs) capability. As a result, it is possible to create nanoscale MIM waveguides such as power splitters/ combiners [8-9], couplers [10-11], interferometers [12]. All these considered promising candidates for future plasmonic devices with their nanometric sizes [13-14].

Rather than conventional split ring geometry, square ring resonator geometry with MIM configuration is demonstrated for THz or optical frequencies applications in [15-16]. In terms of the improved Q-factor, the SRR outperformed the linear resonator because of the obvious advantages of the effects of open-end. Integrated electronic devices require optical excitation, electronic tuning, electronic switching etc. Several structural geometries based on MIM configurations have been studied and numerically analyzed using coupled mode theory (CMT) [17].

This paper reports the study of the dual-band and triple-band SRR using distributed transmission line model. The SRR transmitted modes at an optical frequency range at optical bands (O and L). Both the filtering characteristics and transmission characteristics of the SRR are studied by the full-wave simulation method. It is observed that the resonant modes can be adjusted by manipulating the radius of the SRR. The designs can minimize the filter dimensions and other important optical applications in the PIC. The simulation and analysis are carried out using Finite Differential Time Domain (FDTD) based solver known as CST Microwave studio suite. The wave port is used for excitation in MIM waveguide, Dual-band SRR and Triple-band SRR.

Section II describes the Basic MIM waveguide characteristics in terms of effective refractive Index (Neff) and propagation length (PL). In Section III and Section IV, the characteristics of band-pass filters like transmission and insertion losses of the Dual-band SRR and triple-band SRR have been described. Finally, some conclusions about band-pass filter characteristics in nano-scale MIM wave guiding structures are concluded in Section V.

II. MIM WAVEGUIDE DESIGN AND ANALYSIS

Figure 1 (a) represents the schematic diagram of the MIM waveguide structure with two metal slabs and one dielectric slab. Silica (SiO2) is used as a dielectric material at the interface of the two metal layers with a dielectric constant $\varepsilon SiO2 = 2.50$ [18], and the silver is used as a metal. The silver dielectric properties can be adopted by using the Drude model [19]:

$$\varepsilon(m) = 1 - \frac{\omega_p^2}{\omega\left(\omega + i\gamma_p^2\right)}, \qquad (1)$$

where $\omega_p = 1.38 \times 10^{16}$ rad/sec and $\gamma_p = 2.73 \times 10^{13}$ rad/sec. Figure 1 (b) shows the equivalent distributed lumped model for MIM waveguide for single conductor standard transmission line.

(a)

(b)
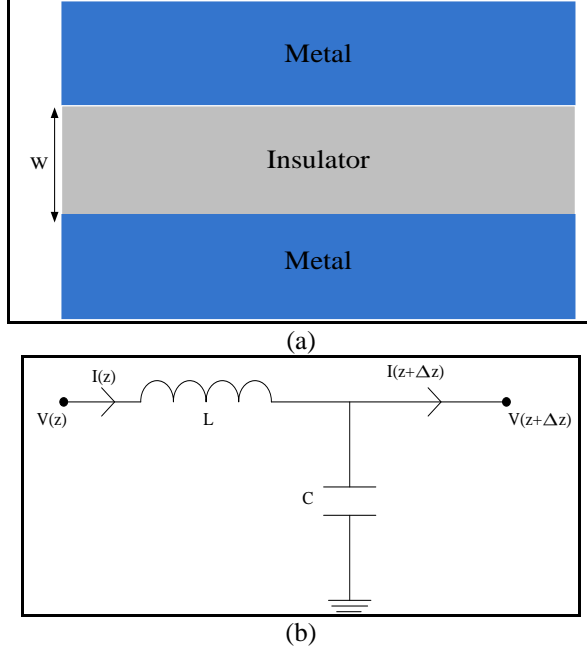
Fig. 1. (a) Basic MIM waveguide structure with two metal slabs with silica (SiO₂) insulator, and (b) distributed circuit for MIM waveguide.

The MIM waveguide supports the TM wave propagation and the field components can be calculated using Maxwell equations as:

$$E_x = -iA\frac{1}{\omega\varepsilon_0\varepsilon_1}k_1 e^{i\beta x}e^{k_1 z} + iB\frac{1}{\omega\varepsilon_0\varepsilon_1}k_1 e^{i\beta x}e^{-k_1 z},$$

$$E_z = A\frac{\beta}{\omega\varepsilon_0\varepsilon_1}e^{i\beta x}e^{k_1 z} + B\frac{\beta}{\omega\varepsilon_0\varepsilon_1}e^{i\beta x}e^{-k_1 z},$$

$$H_y = Ae^{i\beta x}e^{k_1 z} + Be^{i\beta x}e^{-k_1 z}. \qquad (2)$$

Here β is a propagation constant of a MIM waveguide and $k_1 = \sqrt{\beta^2 - k_0^2}$ is the wave-vector perpendicular to the propagation direction (k_0 is the propagation constant of free space).

The wavevector of SPPs in MIM waveguide is given by $k_{sp} = \left(2\pi/\lambda_o\right)\left[\varepsilon_m\varepsilon_i/\left(\varepsilon_m + \varepsilon_i\right)\right]^{1/2}$. Here λ_o is the

wavelength in air, ε_m is dielectric constant of metal and ε_i is the dielectric constant of insulator.

The gap dispersion relation can be written as

$$\tanh\left(\sqrt{\beta^2 - k_0^2\varepsilon_i}.w/2\right) = -\frac{\varepsilon_i\sqrt{\beta^2 - k_0^2\varepsilon_m}}{\varepsilon_m\sqrt{\beta^2 - k_0^2\varepsilon_i}}.$$ W is the

width of the insulator, $\mathrm{Re}(\beta)$ is the phase velocity of SPP in the insulator slit and $\mathrm{Im}(\beta)$ is the energy loss, effective mode index of the gap SPP is $N_{eff} = \mathrm{Re}(\beta)/k_0$ and propagation length (PL) of the MIM waveguide is expressed as $\left[2\,\mathrm{Im}(\beta)\right]^{-1}$.

The propagation constant of gap SPPs is expressed as [20]:

$$\beta \approx k_{sp}\sqrt{1 - \frac{4\varepsilon_i\varepsilon_m}{\varepsilon_m^2 - \varepsilon_i^2}\exp\left(-\alpha_0\sqrt{1 + \frac{4\varepsilon_m^2}{\varepsilon_m^2 - \varepsilon_i^2}\exp\left(-\alpha_0 W\right)}.W\right)},$$

where $\alpha_0 = \sqrt{k_{sp}^2 - \varepsilon_i k_0^2}$.

$$Z_0 = \frac{\beta.W}{\omega.\varepsilon_i},$$ Z_0 is the characteristic impedance, W

is the width of the Insulator, and ω is the angular frequency. βL of the MIM waveguide (L is length of the MIM waveguide) is plays a dominant role in phase shift:

$$t_d = \frac{L}{v_p} = \frac{L}{c}n_{eff}. \qquad (3)$$

Here t_d is the time delay of MIM waveguide for transmitting the signal from port 1 to port 2. Phase shift corresponding to a time delay is $\varphi = \omega t_d$.
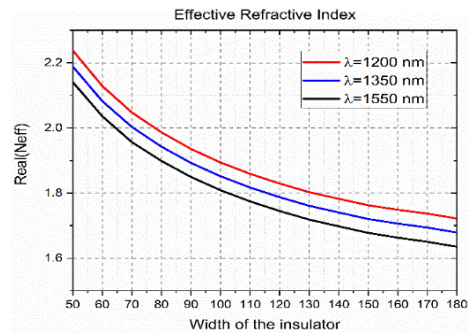
Fig. 2. Real part of N_eff as a function of width of the insulator.

The effective refraction index ($\mathrm{Re}(N_{eff}) = \beta/k_0$)

for three wavelengths (1200 nm, 1350 nm and 1550 nm) by varying width of the insulator is represented in Fig. 2. The propagation length ($L_{SPP} = 1/2 \, \text{Im}(\beta)$) as a function of width of the dielectric is simulated at three wavelengths (1200 nm, 1350 nm and 1550 nm) are represented in Fig. 3. In the plot, the PL is varied between (20-50) µm for a corresponding insulator width in the range of 50 nm to 180 nm. It is possible to infer from Fig. 3 that, as the width of the insulator increases N_{eff} of the MIM waveguide will decrease. The thickness of the silver and SiO2 taken as 50 nm.
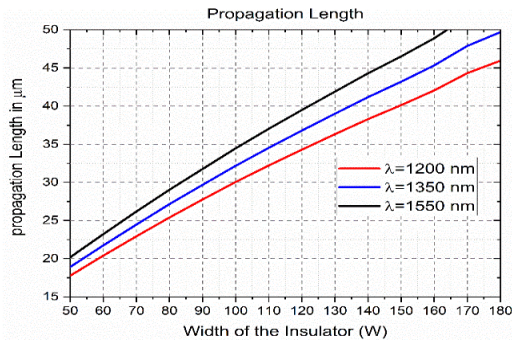
Fig. 3. Propagation length vs width of the insulator at various wavelengths.

III. DESIGN AND ANALYSIS OF DUAL BAND SRR - BPF

Figure 4 (a) represents the schematic diagram of the Dual-band SRR based BPF; these are composed of plasmonic MIM waveguides and a ring resonator. The transmission properties of the MIM waveguide have been studied by using the full-wave Electromagnetic simulation method. The perfectly matched layer (PML) boundary conditions have been used along x and z directions. The mesh sizes are taken as 5 nm x 5 nm, and these are sufficient for numerical convergence. The lumped model for the SRR is represented in Fig. 4 (b).

The width (W3) of the dielectric is smaller than the operating wavelength, due to that only TM mode of propagation can exist in the MIM waveguide. The generated SPPs at the input port (port 1), part of EM waves, will be reflected at the interface of two metal slabs, the remaining portion of the EM waves coupled to the cavity of the small width of the gap. The transmitting and reflecting EM waves in the cavity form the standing waves. These standing waves, coupled at the output port (port 2). The rectangular ring cavity resonance condition is given by [21]:

$$\lambda_m = \frac{\lambda_0}{(\beta_g / \beta_0)} = \frac{l_1 + l_2}{m}, \qquad (4)$$

where m = 0,1,2,3……, and (β_g/β_0) is the normalized propagation constant, λ_0 is fundamental wavelength.

The overall length of the SRR can be calculated from $L = N\lambda_g = N(\lambda_0 / \text{Re}(n_{eff}))$ where $N = 1,2,3,\ldots$ The first resonance and second resonances valleys are observed at 1600 (N=1) and 1300 (N=2) nm respectively. The effective refractive index at 1300 nm and 1600 nm are 2.1464 and 2.07 respectively. From the above equation, the effective length of the resonator is 772.94 and 1211.28 nm respectively. The optimized length for the square ring resonator for the proposed design is 980 nm.
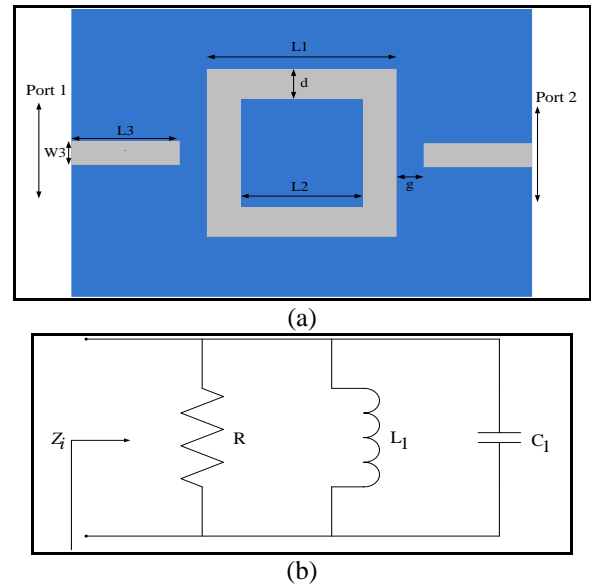
Fig. 4. (a) Dual band SRR-BPF, and (b) distributed model for dual band SRR.

The transmission characteristics of the MIM waveguide-based SRR have been carried out using a commercially available FDTD solver-based CST microwave studio suite under PML boundary conditions with the fixed widths of the waveguide and cavity respectively. L = 980 nm (4*L1) is the total length of the SRR with individual dimensions L_1 = 245 nm, L_2 = 145nm, d = 50 nm, g = 10 nm, W3 = 50 nm and L3 = 100 nm as shown in Fig. 4. The reflection and transmission coefficients are measured in dB throughout the paper. The odd mode analysis of dual-band SRR is giving good results than even mode analysis.

Figure 5 and Fig. 6 represent the transmission characteristics of the proposed device of SRR for length (L) and gap (g) as a function of wavelength. Figure 7 shows the magnetic field distribution at 1300 nm and 1600 nm wavelengths, respectively. The energy of the SPP wave at resonance wavelengths shows stronger coupling of the Dual band BPF.
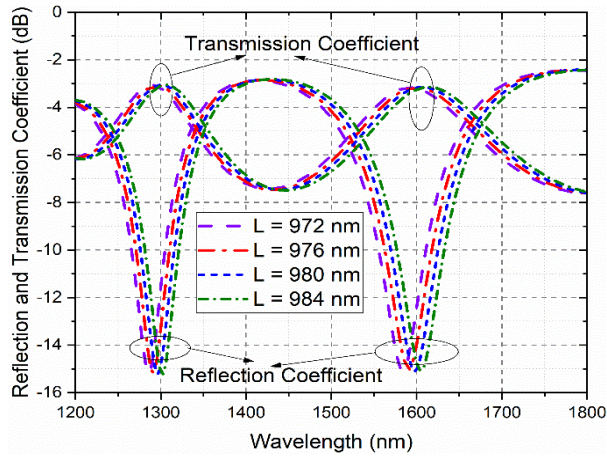
Fig. 5. Reflection and transmission coefficients of dual band SRR-BPF by varying overall length (L) of the square ring.
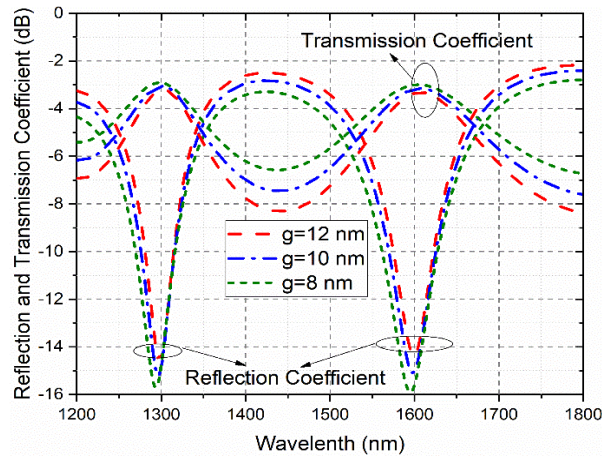
Fig. 6. Reflection and transmission coefficients of dual band SRR-BPF by varying gap (g).

(a)

(b)
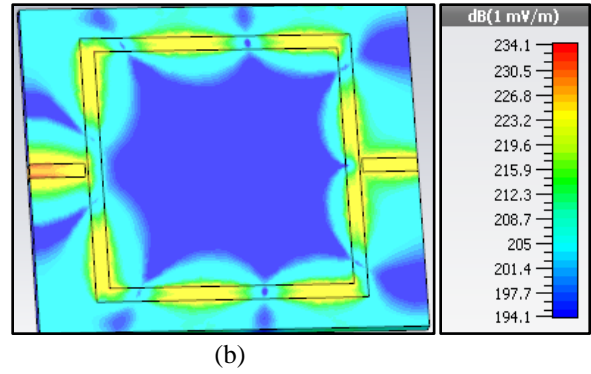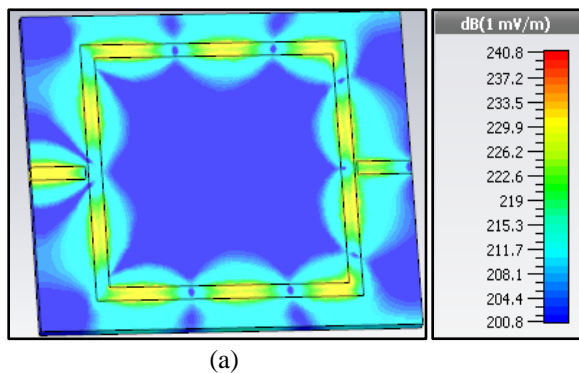
Fig. 7. Field distribution at: (a) 1300 nm (230.6 THz), and (b) 1600 nm (187.37 THz).

IV. DESIGN AND ANALYSIS OF TRIPLE BAND SRR-BPF

To obtain triple band pass response based on the dual band filter layout, additional four open stubs are added on the four sides of the SRR represented in Fig. 8 (a). The length of the stub is L3 = $\lambda_g/4$ where λ_g is the guided wavelength. The optimized length of the open-ended stub is 350 nm. By including the stub in the dual-band SRR the performance of filter improves in operating to triple bands. The slot width and length are adjusted to get the better operating bands. The optimized dimensions of the proposed triple-band SRR-BPF are L1= 1050 nm, W1= 50 nm, L4=100 nm, W4=50 nm, L2= 950 nm, L3= 350 nm, g= 10 nm and W3 = 50 nm. The designed triple-band BPF is simulated under PML boundary conditions. The obtained simulation results show that the proposed filter gives triple operating bands. The operating bands are 1201 nm (249.6 THz), 1354 nm (221.4 THz), and 1544 nm (194.16 THz). The lumped model for triple band SRR is represented in Fig. 8 (b).

(a)

(b)
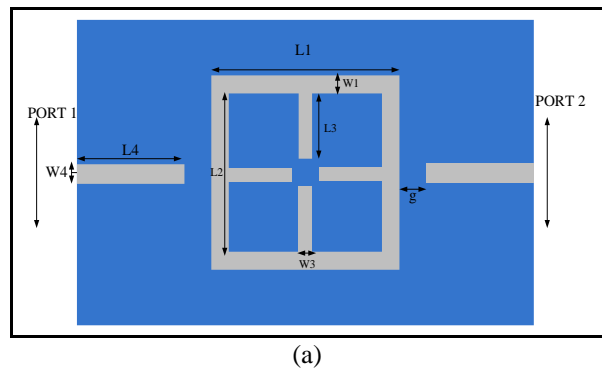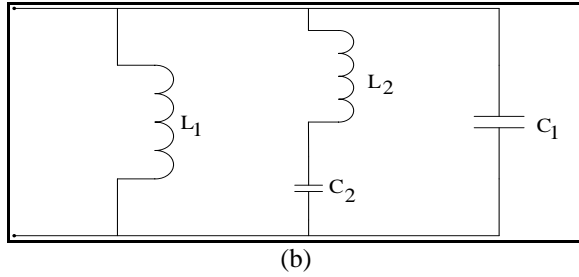
Fig. 8. (a) Triple band SRR-BPF, and (b) distributed model for triple band SRR.

Figure 9 shows the transmission and reflection coefficient of the triple-band SRR-BPF by varying the side length (L1) of the square ring, the best value for the L1 is 1050 nm.

Figure 10 shows the varying L3 parameter (vertical strip length) length from 345 nm to 355 nm by incrementing the 5 nm length. With the increase in length, the resonant valley is moved from higher to lower wavelengths. The optimized value of L3 is 350 nm. Figure 11 shows the variation of the gap from 8 nm to 14 nm with an increment of 2 nm. As the gap increases, the change in resonant valleys decreased along with bandwidth. Finally, the optimized value for the gap is 10 nm. Figure 12 shows the field distributions at the three resonant frequencies. The energy intensity of the SPP waves is more accumulated on the metal and insulator region of the resonant wavelengths of the triple-band BPF for improving the transmission. According to the simulation results the Odd mode analysis giving better results than even mode analysis of triple band BPF.
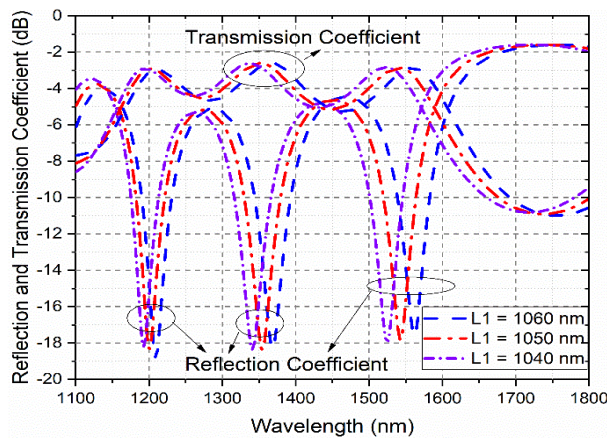
Fig. 9. Reflection and transmission coefficients of triple band SRR-BPF by varying L1.
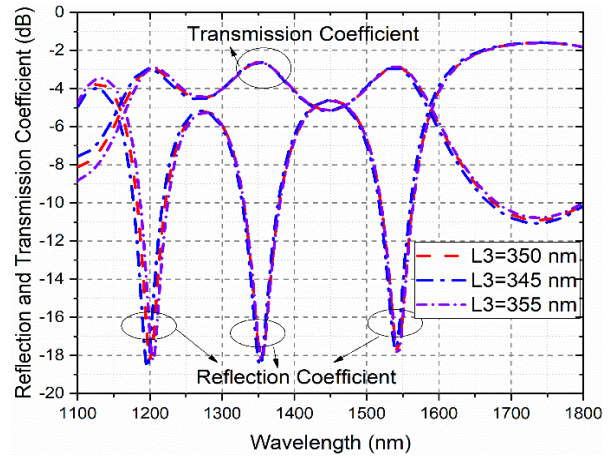
Fig. 10. Reflection and transmission coefficients of triple band SRR-BPF by varying L3.
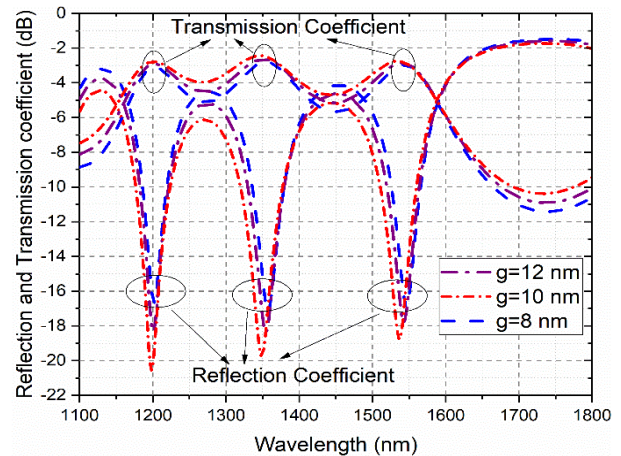
Fig. 11. Reflection and transmission coefficients of triple band SRR-BPF by varying gap (g).

(a) 1201 nm (249.6 THz)

(b) 1354 nm (221.4 THz)
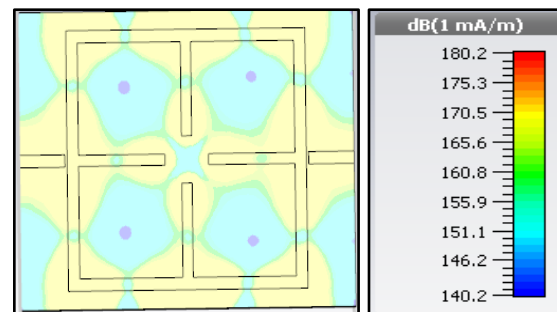
(c) 1545nm (194.16 THz)
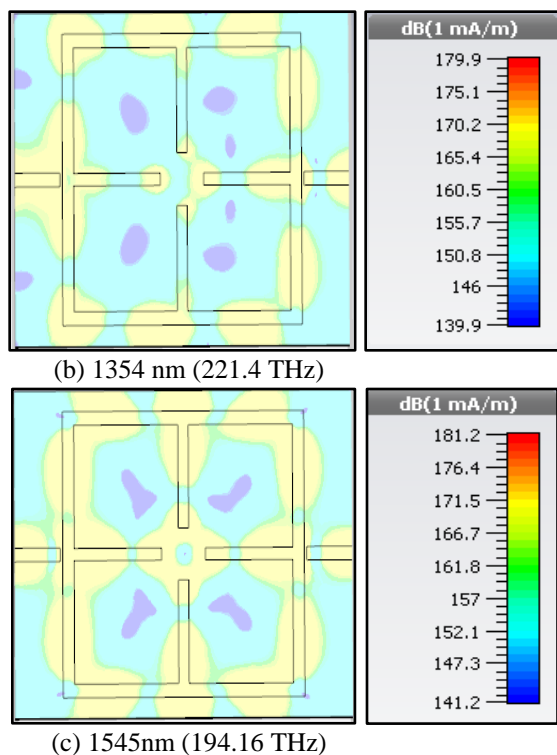
Fig. 12. Field distribution at: (a) 1201 nm, (b) 1354 nm, and (c) 1545 nm.

V. CONCLUSION

In this paper, a novel Nanoplasmonic square ring resonator is designed and investigated. The structure was comprised of a square ring with a MIM configuration. Dual and triple-band characteristics square ring resonators are analyzed with two different designs. The first design with a square ring and resonated at 230.6 THz (1300 nm) and 187.37 THz (1600 nm). Further, the inclusion of four more stubs inside the ring shifted the lower and upper resonant frequencies. Also, it included another intermediate frequency with corresponding resonating frequencies as 1201 nm (249.6 THz), 1354 nm (221.4 THz), and 1544 nm (194.16 THz). Both the designs have excellently contributed to the multi-band characteristics with the corresponding reflection coefficients well below -18 dB for all the resonant frequencies. Further, array configuration development using this basic geometry would be a proper scope of future work.

REFERENCES

[1] N. N. Feng, M. L. Brongersma, and L. Dal Negro, "Metal-dielectric slot-waveguide structures for the propagation of surface plasmon polaritons at 1.55 µm/m," *IEEE J. Quantum Electron.*, vol. 43, no. 6, pp. 479-485, 2007.

[2] H. A. Jamid and S. J. Al-Bader, "Reflection and transmission of surface plasmon mode at a step discontinuity," *IEEE Photonics Technol. Lett.*, vol. 9, no. 2, pp. 220-222, 1997.

[3] H. A. Jamid and S. J. Al-Bader, "Diffraction of surface plasmon-polaritons in an abruptly terminated dielectric-metal interface," *Technology*, vol. 7, no. 3, pp. 321-323, 1995.

[4] M. H. El Sherif, O. S. Ahmed, M. H. Bakr, and M. A. Swillam, "Polarization-controlled excitation of multilevel plasmonic nano-circuits using single silicon nanowire," *Opt. Express*, vol. 20, no. 11, pp. 12473-12486, 2012.

[5] I. Liberal, I. Ederra, R. Gonzalo, and R. W. Ziolkowski, "Induction theorem analysis of resonant nanoparticles: Design of a Huygens source nano-particle laser," *Phys. Rev. Appl.*, vol. 1, no. 4, pp. 1-14, 2014.

[6] S. J. P. Kress, F. V. Antolinez, P Richner, S. V. Jayanti, D. K. Kim, F. Prins, A. Riedinger, M. P. C. Fischer, S. Meyer, K. M. McPeak, D. Poulikakos, and D. J. Norris, "Supplementary information: Wedge waveguides and resonators for quantum plasmonics," *Nano Lett.*, vol. 15, no. 9, pp. 6867-6275, 2015.

[7] Q. Zhang, X.-G. Huang, X.-S. Lin, J. Tao, and X.-P. Jin, "A subwavelength coupler-type MIM optical filter," *Opt. Express*, vol. 17, no. 9, pp. 7549-7554, 2009.

[8] M. A. Ayad, S. S. A. Obayya, and M. A. Swillam, "Submicron 1xN ultra-wideband MIM plasmonic power splitters," *J. Light. Technol.*, vol. 32, no. 9, pp. 1814-1820, 2014.

[9] Y. Rahbarihagh, F. Kalhor, J. Rashed-Mohassel, and M. Shahabadi, "Modal analysis for a wave-guide of nanorods using the field computation for a chain of finite length," *Applied Computational Electromagnetics Society Journal*, vol. 29, no. 2, pp. 140-148, 2014.

[10] Y. Y. Xie, Y. X. Huang, W. L. Zhao, W. H. Xu, and C. He, "A novel plasmonic sensor based on metal-insulator-metal waveguide with side-coupled hexagonal cavity," *IEEE Photonics J.*, vol. 7, no. 2, pp. 1-12, 2015.

[11] C. H. Du and Y. P. Chiou, "Vertical directional couplers with ultra-short coupling length based on hybrid plasmonic waveguides," *J. Light. Technol.*, vol. 32, no. 11, pp. 2065-2071, 2014.

[12] M. Kashif, A. A. A. Bakar, N. Arsad, and S. Shaari, "Development of phase detection schemes based on surface plasmon resonance using interfero-metry," *Sensors (Basel)*, vol. 14, no. 9, pp. 15914-15938, 2014.

[13] E. Ozbay, "Plasmonics: Merging photonics and electronics at nanoscale dimensions," *Science*, vol. 311, no. 5758, pp. 189-193, 2006.

[14] N. H. Fouad, A. O. Zaki, D. C. Zografopoulos, L. A. Shahada, R. Beccherelli and M. A. Swillam,

"Hybrid plasmonic conductor-gap-silicon microring-on-disks electro-optic modulator," *ACES Conference*, 2017.

[15] M. Zavvari, M. T. H. Azar, and A. Arashmehr, "Tunable band-stop plasmonic filter based on square ring resonators in a metal-insulator-metal structure," *J. Mod. Opt.*, vol. 64, no. 20, pp. 2221-2227, 2017.

[16] J. Wen, J. Chen, K. Wang, B. Dai, Y. Huang, and D. Zhang, "Broadband plasmonic logic input sources constructed with dual square ring resonators and dual waveguides," *IEEE Photonics J.*, vol. 8, no. 2, pp. 1-9, 2016.

[17] C. Min and G. Veronis, "Absorption switches in metal-dielectric-metal plasmonic waveguides," *Opt. Express*, vol. 17, no. 13, pp. 10757-10766, 2009.

[18] E. D. Palik, *Handbook of Optical Constants of Solids*. New York, NY, USA: Academic, 1985.

[19] S. A. Maier, *Plasmonics*: *Fundamentals and Applications*. Springer Science, 2007.

[20] S. I. Bozhevolnyi and T. Sondergaard, "General properties of slow-plasmon resonant nanostructure: Nano-antennas and resonators," *Opt. Exp.*, vol. 15, no. 17, pp. 10869-10877, 2007.

[21] B. Yun, G. Hu, and Y. Cui, "Theoretical analysis of a nanoscale plasmonic filter based on a rectangular metal-insulator-metal waveguide," vol. 43, no. 38, pp. 385102, 2010.

Surendra Kumar Bitra received M.Tech degree from K L University in 2012. He is presently working as a Research Scholar in Koneru Lakshmaiah (KL) University, Guntur, India. His research area is Plasmonics, Nano Photonics and Nanoplasmonic devices.

M. Sridhar received Ph.D. degree from JNTU Kakinada, Kakinada, India in 2017 and M.Tech degree from Jawaharlal Nehru Technological University, Anantapur, India in 2009. He is a Senior Member of Institute of Electrical and Electronics Engineers (IEEE) and The Institution of Electronics and Telecommunications Engineers (IETE). He is presently working as a Professor in Koneru Lakshmaiah (KL) University, Guntur, India. His area of interest is developing ionospheric scintillation mitigation algorithms and satellite communications. He is having 19 years of teaching experience. He has published his research papers in 16 International Journals and 5 International/National Conferences. He is one of the members of IRNSS/NAVIC project from KL University in collaboration with Space Applications Centre (SAC), Ahmedabad, Indi.